minerals

MDPI

Article

Holocene Lacustrine Abiotic Aragonitic Ooids from the Western Qaidam Basin, Qinghai-Tibetan Plateau

Yongjie Lin [1], Ian M. Power [2] and Wenxi Chen [1,*]

[1] Key Laboratory of Saline Lake Resources and Environments of Ministry of Natural Resources, Institute of Mineral Resource, Chinese Academy of Geological Sciences, Beijing 100037, China
[2] Trent School of Environment, Trent University, 1600 West Bank Drive, Peterborough, ON K9L 0G2, Canada
* Correspondence: chenwenxi@mail.cgs.cn

Abstract: Carbonate ooids are a significant component of shallow water carbonate deposits in the present and geologic past, yet their origin and formation mechanism have been the subject of continuing debate. This study focuses on the well-preserved Holocene aragonitic ooids collected from the west Qaidam Basin, Qinghai-Tibetan Plateau (QTP). The mineralogical and chemical compositions, and stable ($\delta^{13}C$ and $\delta^{18}O$), and radiocarbon isotopes of the ooids were analyzed to investigate their formation and develop a depositional model. The ooids formed approximately 5377 ± 61 cal BP, and their cortices were composed of microcrystalline aragonite, with most nuclei being quartz grains. Stable carbon and oxygen isotopes indicate that authigenic aragonite precipitation is driven by evaporation and associated degassing of CO_2 under turbulence conditions in a shallow alkaline lakes. Furthermore, eletron microscopy showed no presence of microfossils in ooid cortices or other evidence of microbial activity. Therefore, we propose that aragonite precipitation during ooid formation is most likely induced abiotically by increasing alkalinity due to evapoconcentration of lake waters based on an absence of an efficient carbonate-inducing metabolic pathway. New observations and detailed analyses of aragonitic ooid samples in the Qaidam Basin provide an improved understanding of the origin and formation processes of carbonate ooid in modern environment and the geologic past.

Keywords: ooids; aragonite; lacustrine; abiotic origin; holocene; Qaidam basin

check for updates

Citation: Lin, Y.; Power, I.M.; Chen, W. Holocene Lacustrine Abiotic Aragonitic Ooids from the Western Qaidam Basin, Qinghai-Tibetan Plateau. *Minerals* **2022**, *12*, 1400. https://doi.org/10.3390/min12111400

Academic Editors: Vincent V. Barbin and Frédéric Marin

Received: 17 September 2022
Accepted: 27 October 2022
Published: 31 October 2022

Publisher's Note: MDPI stays neutral with regard to jurisdictional claims in published maps and institutional affiliations.

Copyright: © 2022 by the authors. Licensee MDPI, Basel, Switzerland. This article is an open access article distributed under the terms and conditions of the Creative Commons Attribution (CC BY) license (https://creativecommons.org/licenses/by/4.0/).

1. Introduction

A carbonate ooid is a small (commonly < 2 mm in diameter) subspherical or spherical particle with an internal concentric structure. Ooids are found globally in a variety of settings, including alkaline lakes [1–6] and marine environments from the Precambrian onward [7–9]. They are usually composed of calcium carbonate (calcite or aragonite), which has attracted great interest due to their importance as a carbon sink, palaeoclimatic/palaeoeanographic indicators, and potential reservoirs for hydrocarbons [2,4–6]. The formation mechanism of carbonate ooids is variable and complex, depending on numerous environmental factors. Therefore, their origin has been the subject of continuing debate, mainly focusing on their abiotic or biochemical origin [10–14]. Various hypotheses have been reported on the genesis of carbonate ooids, including (i) solely abiotic processes mediated by physiochemical factors [11,15]; (ii) biogenic processes involving microbial extracellular polymeric substances (EPS) [13,15]; and (iii) microbial mats that influence calcium carbonate saturation through alteration of carbonate alkalinity and Ca^{2+} availability [12,16,17]. Generally, the biogenic formation mechanism suggests that microbes play a constructive role in precipitating or inducing carbonate precipitation [10,12,13,18]. On the contrary, the abiotic formation mechanism suggests that microorganisms or organic compounds do not play a primary role in carbonate ooids precipitation [11,15,19]. Consequently, the processes involved in aragonitic ooids formation in nature are the subject of debate.

Lacustrine carbonate ooids have attracted greater scrutiny than marine ooids due to their limited scale [2,4–6]. Holocene lacustrine carbonate ooids widely occur in the playas of western Qaidam Basin, the largest intermontane basin in the northeast Qinghai-Tibetan Plateau (QTP). In their study of these ooids, Sun et al [20] reported the clear signals of scytonemin from ooid, a unique cyanobacterial ultraviolet radiation (UVR)-shielding pigment, and this biomarker may be an indication of the depositional environment. However, the origin and formation mechanism of the Holocene carbonate ooids in the western Qaidam Basin is still poorly understood, and especially the role of microbes is unknown.

To assess the origin and formation process of ooids, we examined the Holocene lacustrine carbonate ooids in Qaidam Basin. We used an integrated approach involving isotopes, trace elements, microscopy, and fluorescence analysis to investigate the origin of carbonate ooids and assess if microbes have a constructive role in their formation. Our results provide new insights into the origin and formation condition for aragonitic ooids with implications for improving their interpretation in the geologic record.

2. Geological Setting

The Qaidam Basin is the largest intermontane sedimentary basin along the northeastern Tibetan Plateau (Figure 1) with an area of 120,000 km^2 and average elevation of 3000 m [21]. The basin is almost entirely an area of interior drainage by ongoing India–Asia collision since the early Oligocene [22]. Presently, the basin is triangular-shaped and is bordered by three large faults, the Kunlun Fault to the south, the Altyn Tagh Fault to the west, and the Qilian Fault to the north [22]. Nearly one quarter of the basic covered by playas and salt flats. The Qaidam Basin preserves Cenozoic sedimentary successions since early Eocene with a thickness of around 12 km. The early–middle Miocene strata are composed of the Xiayoushashan and Shangyoushashan Formations [23]. Holocene carbonate ooids widely occur in the west Qaidam Basin [20] including in the studied Honggouzi section located on the northwest of Qaidam Basin (Figure 1; 38°27′43.12″ N; 91°16′47.93″ E). This study area hosts a large succession of Cenozoic sedimentary rocks that are composed of mudstone, sandstone, marl, limestone, and gypsum [21].

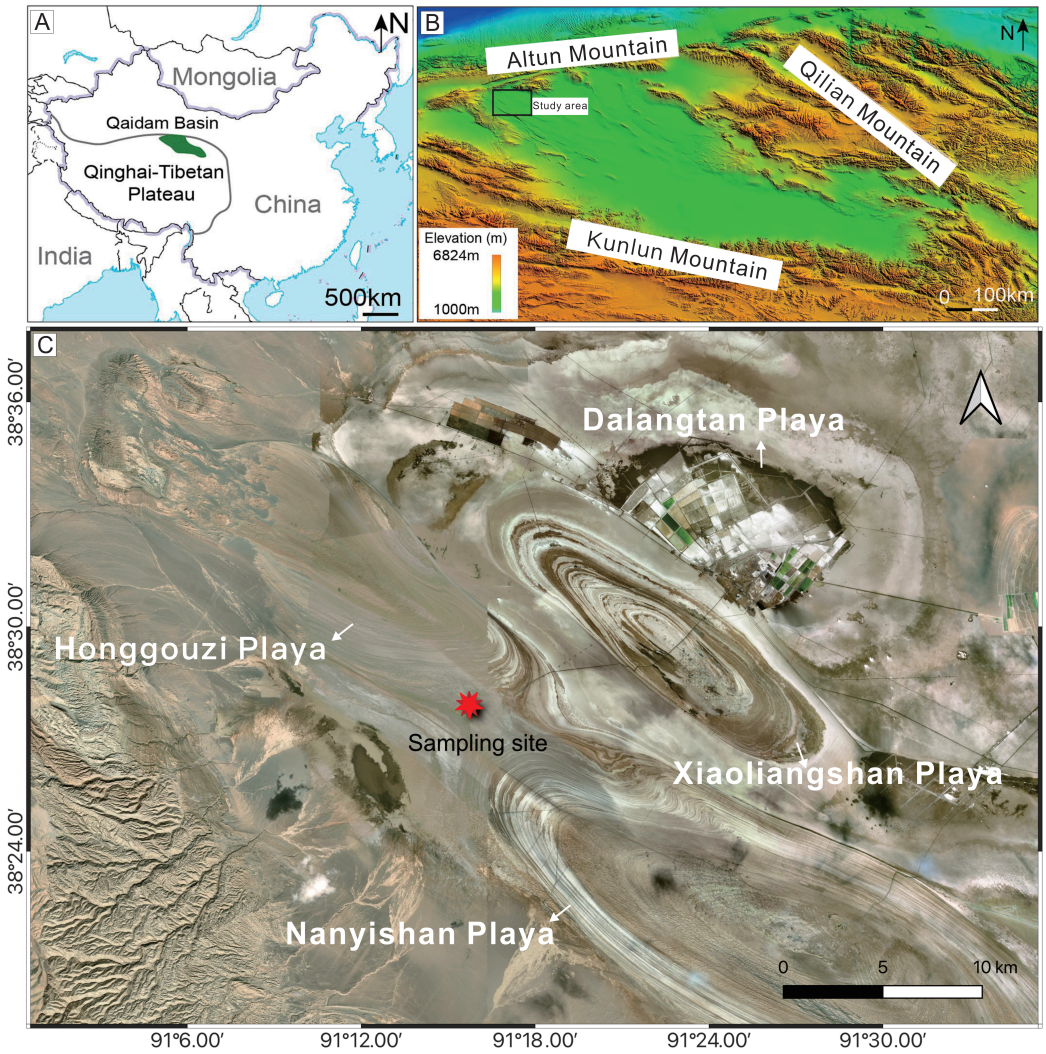

Figure 1. (**A**) The location of the Qaidam Basin in QTP; (**B**) digital elevation model map of the Qaidam Basin; (**C**) satellite map of the study area.

3. Materials and Methods

3.1. Sampling

Holocene lacustrine carbonate ooids widely occur in the west Qaidam Basin [20], and three samples were collected from ooid-bearing layer in the Honggouzi area, western Qaidam Basin (Figure 1; 38°27′43.12″ N; 91°16′47.93″ E). The ooids layer is generally present near the surface, which is currently overlaid by chemical-eolian deposit and underlaid by the lake sediments such clays, carbonate, and evaporites (Figure 2). The ooid-bearing lamina consists of loose ooid sand that is subparallel to the land surface with 2 cm thickness. Three ooid samples were collected from the ooid-bearing lamina.

3.2. Microscopy and X-ray Diffraction Analyses

Petrographic investigations of the ooids were carried out at the China University of Geosciences (Beijing) using a Zeiss Axio Scope A1 microscope fitted with a Leica DMI3000 fluorescence analysis system using UV (excitation wavelength = 365 nm), blue light (excitation wavelength = 450–490 nm), and green light (excitation wavelength = 546 nm) that enabled the identification of organic matter in the ooid cortices. Ultrastructures were determined using scanning electron microscopy (SEM) with element analysis by energy dispersive spectroscopy.

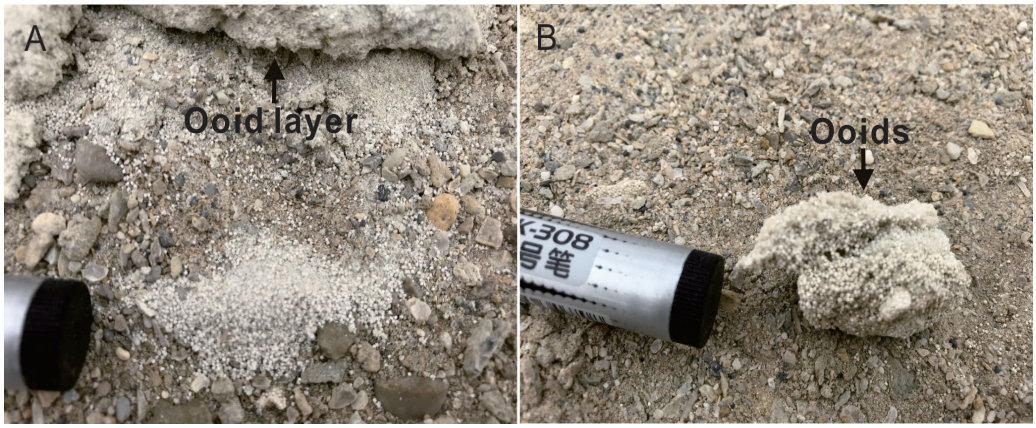

Figure 2. (**A**) Photograph showing the ooid layer in the west Qaidam Basin in QTP; (**B**) photograph showing ooid aggregates (marker for scal, diameter of cap is ~15 mm). The ooids range in size from 200 to 600 µm.

For SEM, ooids were embedded using Buehler EpoThin^{TM}2 epoxy resin and hardener and polished using a Buehler EcoMet30 polisher. The final polish was performed using a TriDent^{TM} pad and MasterPrep^{TM} diamond suspension (0.05 µm). Samples were acid-etched to reveal any potential features (e.g., entombed microbial cells) below the carbonate surface. The details of this method are described by Power et al. [24]. All samples were coated using a Filgen osmium coater (OPC 80T) that applied 10 nm of osmium metal to the sample surface to improve conductivity. An LEO 1540 XB field emission SEM collected high-resolution micrographs at an operating voltage of 1.0 kV. SEM was performed at the University of Western Ontario at the Nanofabrication Facility in London, Ontario, Canada.

X-ray diffraction (XRD) analyses were performed to determine the mineralogical composition of the ooids. Finely powered ooid samples (200 mesh-sized sieve) were analyzed at the Institute of Mineral Resources, Chinese Academy of Geological Sciences, using a Rigaku MiniFlex 600 X-ray diffractometer under the operating conditions of $Cu - K\alpha$ radiation (40 kV and 30 mA). Data were collected continuously from 3° to 70° using a step size of 0.04° and a counting time of 0.8 s/step. Search-match software, MDI Jade XRD software, and the International Centre for Diffraction Data (ICDD) database were used for phase identification. The mineral compositions of the bulk were obtained using Rietveld refinement methods.

3.3. Major and Trace Elements Analyses

Major and minor element compositions of the ooids were measured using X-ray fluorescence (XRF) spectrometry and inductively coupled plasma mass spectrometry (ICP-MS), respectively. Loss on ignition (LOI) was determined by weighing samples before and after 1 h of heating at 1075 ± 25°C. Detailed operating procedures and conditions for XRF and ICP-MS are the same as those described by Yang et al. [25] and Lin et al. [26], respectively. The analysis precision of major element data was better than 0.05%, and its analytical uncertainties of trace elements are better than ±5% (wt.%) and under ±1 % for measuring rare earth elements (REE). The REE data are normalized to Post-Archean Australian Shale (PAAS) [27], and PAAS-normalized anomalies are calculated as follows [28]: $Ce/Ce^* = 2Ce_{SN}/(La_{SN} + Pr_{SN})$, $Eu/Eu^* = 3Eu_{SN}/(2Sm_{SN} + Tb_{SN})$, and $Pr/Pr^* = 2Pr_{SN}/(Ce_{SN} + Nd_{SN})$.

3.4. Stable Carbon and Oxygen Isotopes Analysis

Stable carbon and oxygen isotopes were measured at the Beijing Research Institute of Uranium Geology, Chinese Ministry for Nuclear Industries, using a Finnigan MAT 253 mass spectrometer coupled with a Thermo Finnigan GasBench II (refer to methods in Lin et al. [29]). The finely powdered ooid samples (200 mesh size) were loaded in exetainer vials after being baked at 105 °C for 2 h and flushed with helium for 5 min. Four to five

drops of 99% phosphoric acid (H_3PO_4) were dispensed to each vial that was then shaken and left to react for a minimum of 2 h at 25°C. The isotopic compositions of evolved CO_2 were measured by mass spectrometer in a helium flow [30]. The precision for isotopic measurement of the ooid samples and in-house standards were both <0.1‰ for $\delta^{13}C$ and $\delta^{18}O$. The $\delta^{13}C$ and $\delta^{18}O$ data were reported using the δ notation measured in ‰relative to Vienna Pee Dee Belemnite (VPDB).

3.5. ^{14}C Analysis

The ^{14}C analyses were performed at Peking University using an updated NEC Compact PKUAMS facility. The preparation procedures of carbonate samples for ^{14}C analysis were detailed and are described by Lin et al. [29]. The ^{14}C values are reported as conventional ^{14}C yr after correction for isotopic fractionation and normalization to ^{13}C (−25‰) using the ^{13}C term measured directly with the Accelerator Mass Spectrometry. Calendar dates of ooid samples were calculated using OxCal v4.2 [31]. The quoted age is in radiocarbon years using the Libby half-life of 5568 years and the uncertainties are reported as 1 σ.

4. Results

Mineralogy and Microscopic Features of Ooids

The ooids are composed of 90–97 wt.% aragonite with minor abundances of quartz that are present as terrigenous clasts incorporated into the ooids during their formation (Figure 3 and Table 1). Microscopy of the ooids reveal that their cortices consist of very fine crystals of aragonite, and nuclei are mainly composed of either quartz or carbonate grains, with minor kaolinite and muscovite (Figure 3). Two types of ooids are observed, including concentric ooids and deformed or distorted ooids (Figure 4). The ooids appear not to have been affected by diagenetic modification; thus, their exquisite structures are well preserved. Concentric ooids with peloid nuclei range in size from 200 to 600 µm. The ratio of concentric ooid cortex thickness to the nucleus is >1. The deformed ooids in the ooids layer are rarely observed and are characterized by flattened or elongated ooids (Figure 4). Acid-etching of the ooids and subsequent electron microscopy imaging did not clearly reveal any preserved microfossils, though this does not exclude them from being present (Figure 5). The dark laminae in all ooid samples show intense fluorescence and actively responding to exciting light, but non- and very weak fluorescence within light laminae (Figure 6).

Geochemical Results

The $\delta^{18}O_{V-PDB}$ values of ooid samples range from 6.6 to 7.5‰, corresponding to $\delta^{18}O_{V-SMOW}$ values ranging of 36.7–38.6‰ [32]. The $\delta^{13}C_{V-PDB}$ values of ooid samples are also all highly positive, ranging from 4.6–5‰ with an average of 4.77‰. The exact dates of ooid formation are around 5377 ± 61 cal BP based on radiocarbon dating.

The ooids are mainly composed of CaO with compositions falling within a narrow range of 42.21–43.07% (avg. = 42.54%) (Table 1). The LOI content ranged from 43.65 to 43.92% (avg. = 43.76%). The Si and Na content ranged from 5.61 to 6.18% (avg. = 5.99%) and 2.05 to 2.11% (avg. = 2.09%), respectively. The Al_2O_3, Fe_2O_3, FeO, Na_2O, K_2O, P_2O_5, TiO_2, and MnO concentrations were all lower than 2%. Thus, the element compositions are consistent with the XRD results, which show that the ooid is composed of aragonite with minor quartz.

The concentration of REEs and yttrium (Y) of the acid leachate are given in Figure 7 and Table 2. Overall, the individual REEs concentrations of ooid samples vary from 0.053 to 5.08 ppm. The ΣREE values are from 12.52 to 13.53 ppm with an average of 12.97 ppm, which is lower than that of typical marine carbonate (∼28 ppm) [33]. The PAAS-normalized REE+Y patterns of ooids samples show a similar pattern with the following characteristics: (1) enrichment in the heavy REEs (ΣLREEs/ΣHREEs = 0.77 ∼ 0.84); (2) negligible Ce anomalies (Ce/Ce^* = 0.88 ∼ 0.98); and (3) consistently negative Eu anomalies (Eu/Eu^* = 0.40 ∼ 0.60).

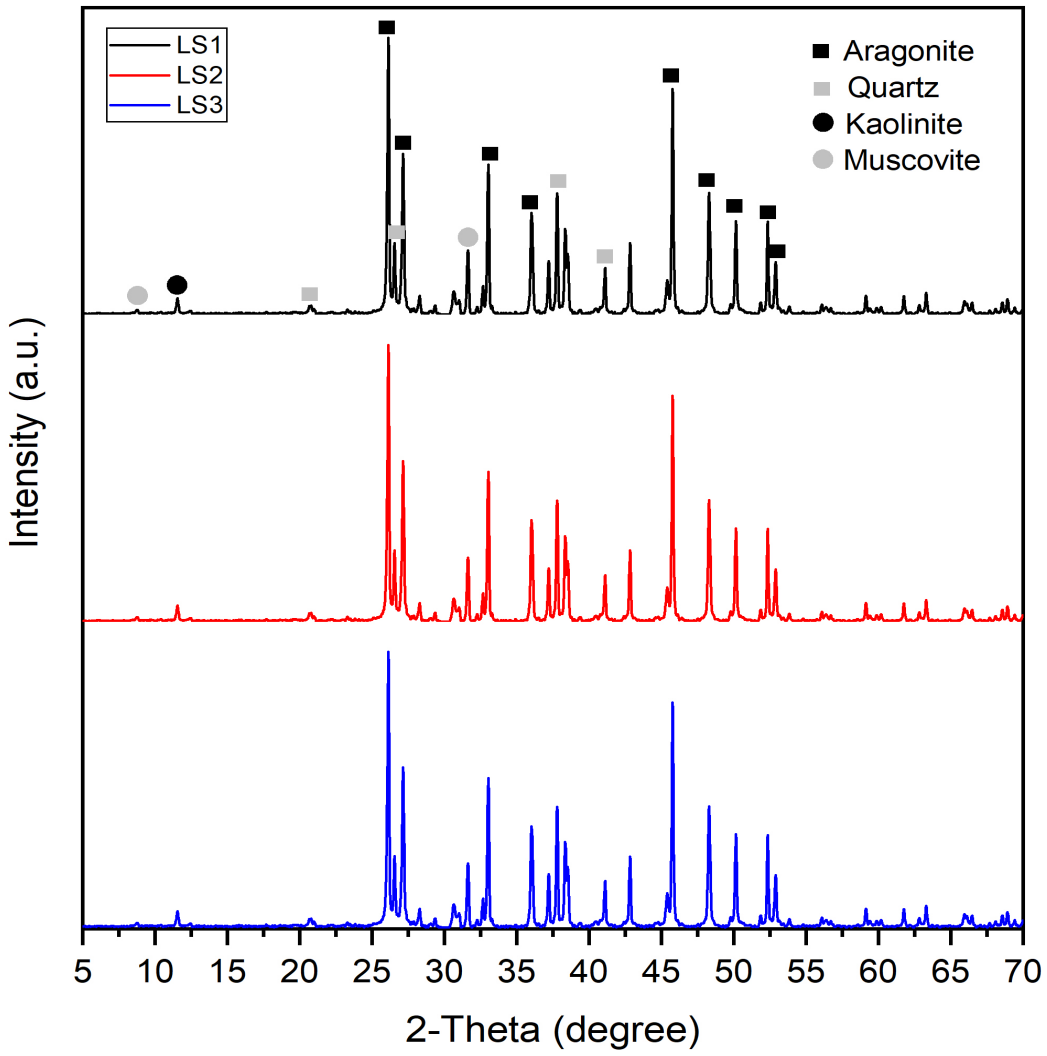

Figure 3. Bulk X-ray diffraction analysis of the three ooid samples.

Table 1. Major element compositions (%) of aragonitic ooids in the western Qaidam basin, QTP.

Sample	SiO_2	Al_2O_3	Fe_2O_3	MgO	CaO	Na_2O	K_2O	MnO	TiO_2	P_2O_5	LOI	FeO
LS-1	6.18	1.06	0.473	2.74	42.35	2.05	0.867	0.011	0.066	0.022	43.71	0.16
LS-2	6.18	1.02	0.456	2.77	42.21	2.11	0.887	0.009	0.06	0.02	43.92	0.2
LS-3	5.61	0.993	0.448	2.62	43.07	2.1	0.87	0.011	0.053	0.022	43.65	0.14

Table 2. REE+Y compositions (ppm) of aragonitic ooids in the western Qaidam basin, QTP.

Sample	La	Ce	Pr	Nd	Sm	Eu	Gd	Tb	Dy	Y	Ho	Er	Tm	Yb	Lu
LS-1	2.19	4.63	0.559	2.01	0.423	0.076	0.300	0.065	0.321	3.500	0.074	0.265	0.043	0.218	0.049
LS-2	2.62	5.08	0.62	2.54	0.528	0.102	0.483	0.093	0.512	3.27	0.104	0.338	0.063	0.385	0.062
LS-3	2.59	4.76	0.61	2.40	0.525	0.067	0.480	0.09	0.462	3.09	0.112	0.315	0.062	0.346	0.059

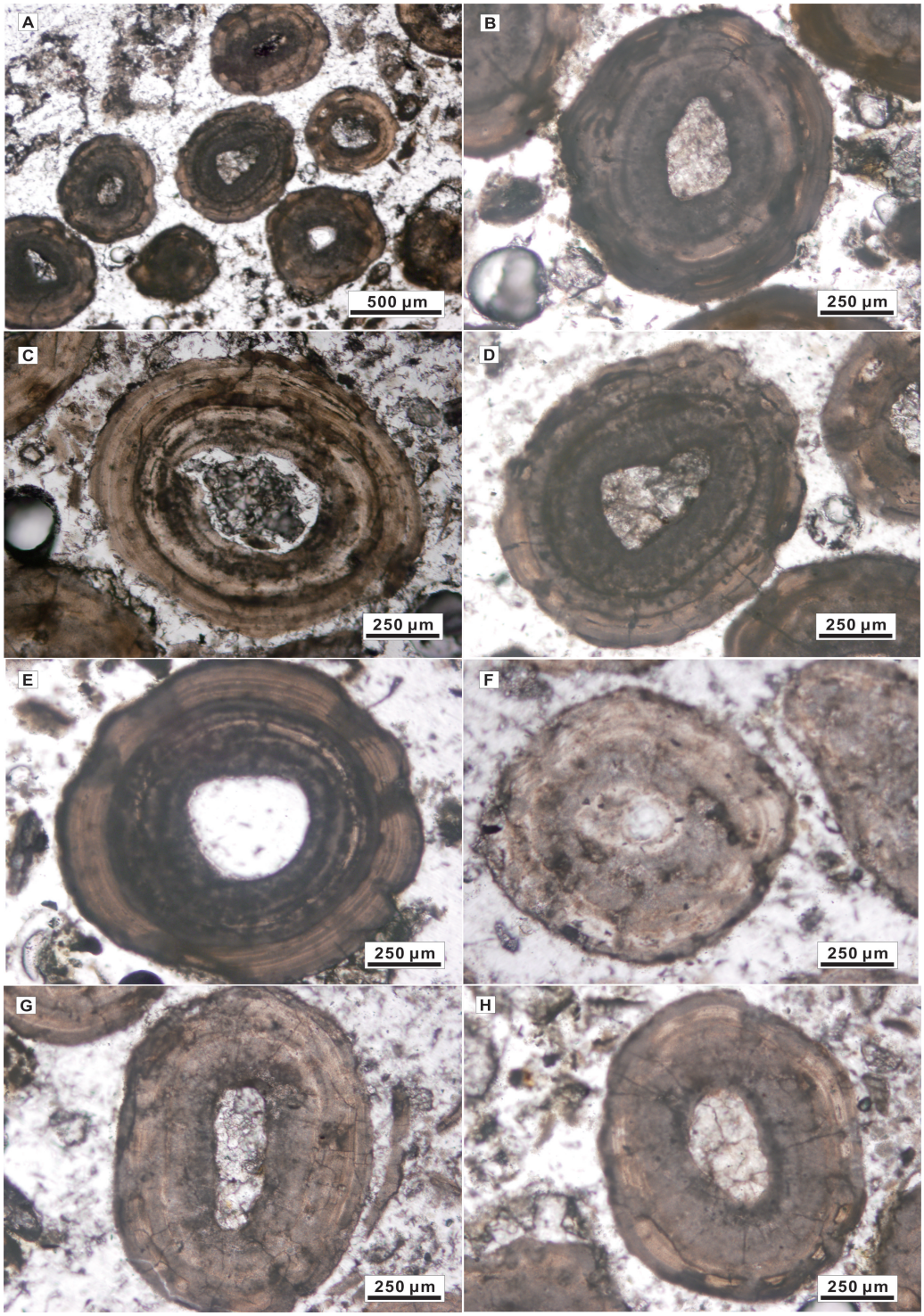

Figure 4. Representative micrographs showing the microscale structure of ooids from petrographic thin section. (**A**–**F**) ooids with a concentric texture; all showing successive laminae that do not thin outward; (**G**,**H**) deformed ooids (i.e., flattened or elongated ooids representing compactional strain).

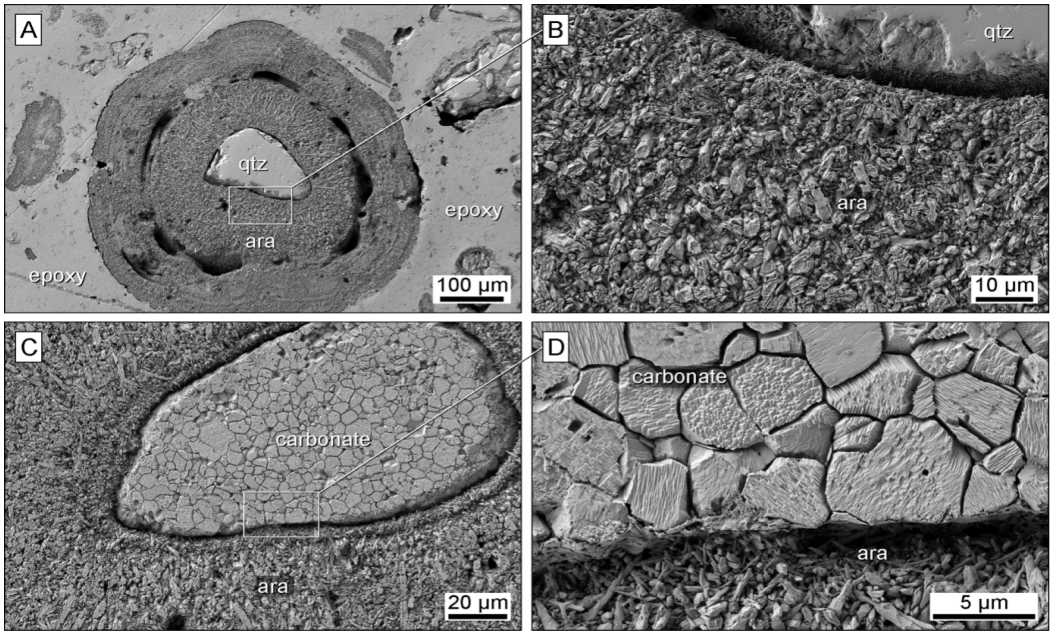

Figure 5. Representative scanning electron micrographs of ooids. (**A**) concentric ooid with a quartz nucleus; (**B**) high magnification view of ooid (**C**) showing the acid–etch surface that reveals the microcrystalline aragonite; (**D**) ooid with a detrital carbonate nucleus at its centre and a high magnification view. There were no clear signs of microfossils within the aragonite cortices (ara denotes aragonite, and qtz denotes quartz).

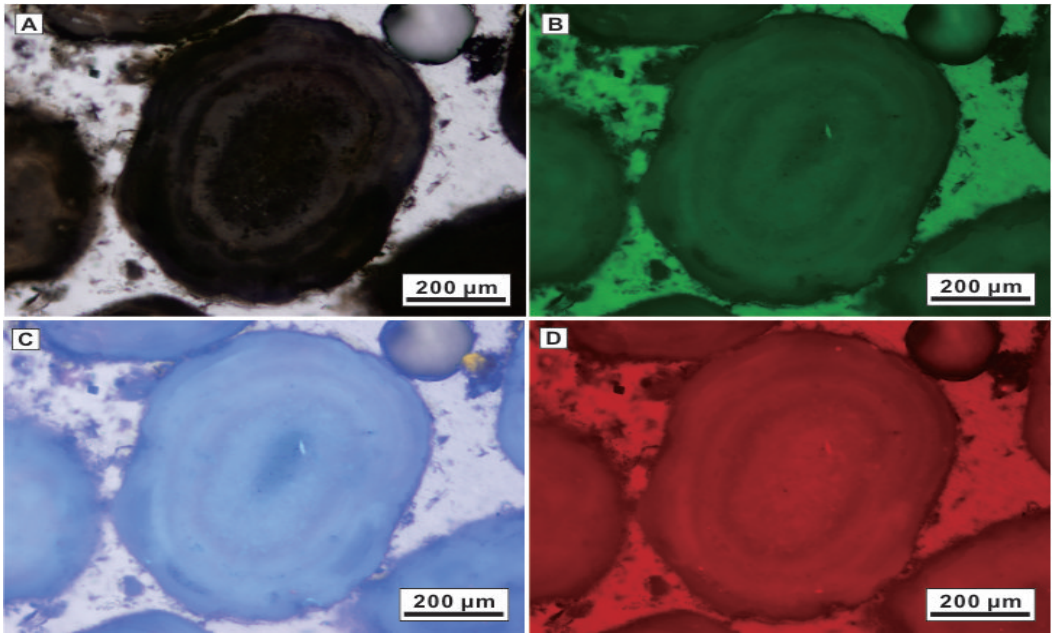

Figure 6. (**A**) Normal light and (**B**–**D**) different wavelengths of fluorescent light under various exciting light wavelengths. Note that dark laminae in ooid samples are actively responding to exciting light wavelengths, reflecting more content of organic matter.

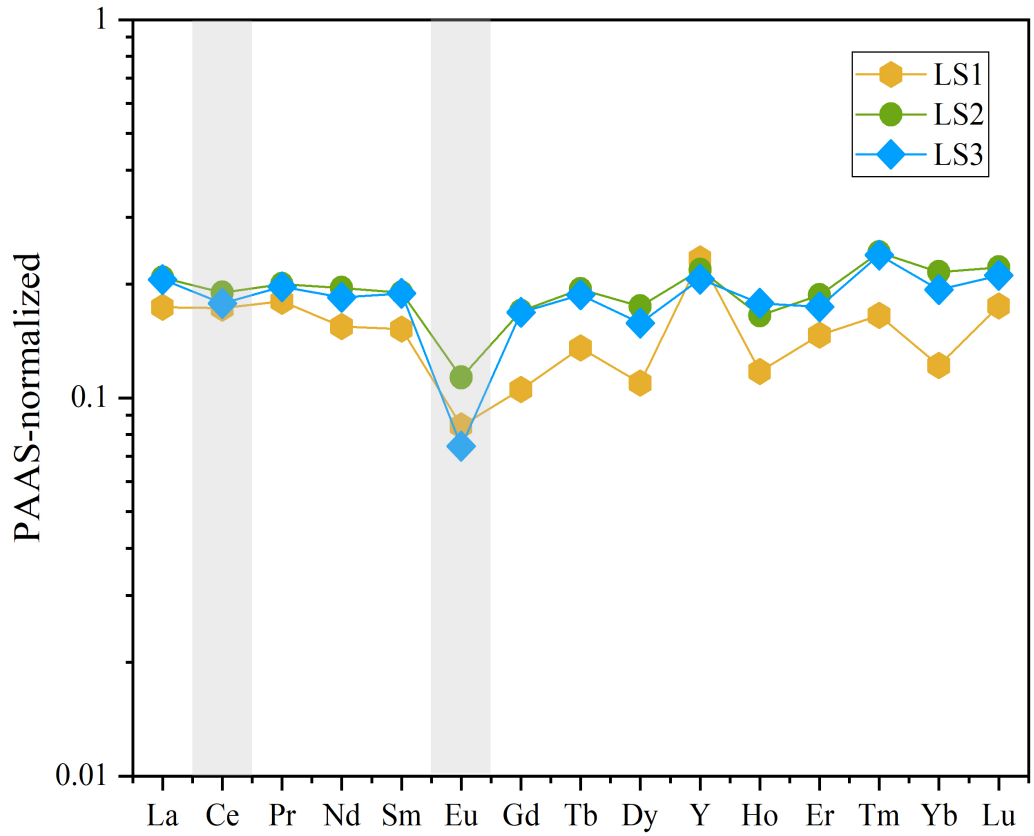

Figure 7. REE+Y patterns of ooids in the western Qaidam basin, QTP.

5. Discussion

5.1. Ooid-Forming Sedimentary Environment

REE compositions of carbonate can preserve modern and ambient aqueous REE signatures, and provide information regarding the environmental conditions in which the carbonates formed [34–36]. In this study, the Holocene aragonitic ooids are well preserved on the surface of a playa with very little burial diagenesis alteration. None of the ooids samples analyzed exhibit bell-shaped REE+Y patterns (Figure 7), and a lack petrographic evidence that would suggest substantial recrystallization; thus, there has been insignificant to no diagenetic alteration on the ooid cortices [36]. Although minor detrital minerals (e.g., kaolinite and muscovite) were observed in the nucleus of ooids, it does not affect the signal of REE that was recorded in aragonite due to the extremely low mineral contents. In addition, the contamination from the admixed terrigenous fractions in aragonitic ooid samples is negligible due to an insignificant relationship between the Ce anomaly and the Mn concentrations in the studied ooids ($R^2 = 0.01$). Therefore, the REE compositions of the Holocene aragonitic ooids reliably represent the REE compositions of the lake waters from which they formed. Rare earth elements exist mostly in a trivalent state except for Ce and Eu, which may also exist as Eu^{2+} and Ce^{4+}, respectively [33,37]. Eu and Ce are sensitive to change in redox conditions and therefore are reliable palaeoredox indicators [38–41]. The Eu and Ce anomalies in natural aqueous systems via redox reactions that can be presented in the following equations:

$$2Eu^{3+} + 2OH^- \rightarrow 2Eu^{2+} + H_2O + 0.5O_2 \quad (1)$$

$$2Ce^{3+} + 3H_2O + 0.5O_2 \rightarrow 2CeO_2 + 6H^+ \quad (2)$$

Eu^{3+} generally dominates except under low temperature, alkaline, and reducing environments at Earth's surface conditions, while Eu^{2+} should predominate in the environment where the temperatures are greater than around 250 °C [42]. Ce^{3+} is oxidized to less sol-

uble Ce^{4+} in oxic conditions, and the precipitated carbonates that precipitate under oxic conditions always exhibit negative Ce anomalies [38,40]. Conversely, carbonates precipitated under reducing conditions always display normal or enriched Ce concentration, and depleted Eu concentration (negative Eu anomalies). Carbonates always display low ΣLREE/ΣHREE ratios in oxic conditions and high ΣLREE/ΣHREE ratios in anoxic conditions due to the light REEs being preferentially removed from oxygenated waters [39,43,44]. Overall, Ce anomalies in carbonates are around 0.4–0.5 for oxic waters and 0.9–1.0 for anoxic waters when used as palaeo-seawater redox proxy [43,45]. In this study, the ooids samples show a significant Eu anomaly, flat REE pattern, and a lack of negative Ce/Ce* anomalies, suggesting that they formed in suboxic to anoxic environments. Otherwise, the Ce/Ce^* values of the ooid samples are higher than the range documented for Holocene microbialites of well-oxygenated shallow water settings [37]. These high Ce/Ce^* and positive Eu/Eu^* values of ooids possibly reflect reducing conditions, and the sedimentary environments that ooid precipitated were not influenced by the hydrothermal activity.

Ooid size (i.e., diameter) and accumulation are mainly controlled by hydrodynamic processes, which is a reliable proxy for hydrodynamic conditions [18,46]. Both empirical observations and experiments indicate that ooids size directly relates to current velocity and that ooids from low energy conditions (e.g., active shoals) are smaller than those from high energy environments [18,19,46–48]. Larger ooids are generally formed under more agitated conditions or over a relatively longer time period [15,18,19,47]. In this study, ooid sizes ranged from 200 to 600 µm, and the nuclei were mainly comprised of quartz grains. In addition, well-formed, well-sorted, cross-bedded ooids may further indicate that the ooid samples form in high-energy depositional conditions [49]. The coarse and fine sand at the lake shore with large waves can be easily stirred up under strong hydrodynamic, and then transient suspension in lake waters, and thus the carbonates can precipitate at the surface of these sands [50]. We conclude that the ooids formed and accumulated during high hydrodynamic periods and reduced lake shore conditions.

5.2. Abiotic Origin of the Ooids

The main question we aimed to ascertain in this study was if the ooids from the west Qaidam Basin had an abiotic or biotic origin. Numerous studies suggest a biologically-mediated process for carbonate precipitation via active and passive mechanisms [13,16,17,51,52]. For example, Diaz et al. [13] proposed that biomediated amorphous calcium carbonate (ACC) precipitation is a key process in ooid formation. This biogenic process involves microbial extracellular polymeric substances (EPS) [13,52], and the nucleation process is controlled by the biological production and degradation of EPS, which is a bigologically-influenced mechanism (aka passive mineralization) [53,54]. Furthermore, a biologically-induced mechanism (i.e., active mineralization; e.g., sulfate-reduction) suggests that the calcitic or aragonitic ooid formation is induced by the metabolic activities and metabolic by-products that affect calcium carbonate saturation, e.g., increases carbonate alkalinity and Ca^{2+} activity [12,13,16,17,52,55,56]. In addition, laboratory experiments have successfully simulated carbonate precipitates in defined spherical microbial communities [51]. However, it is unclear if microbes are required for ooid formation or do not play a role in carbonate precipitation when present.

Duguid et al. [11] found that the ooids from the Bahamian Archipelago contained numerous cement-filled microborings throughout their cortices and that these had an association with two different species of *cyanobacteria*, *Solentia*, and *Hyella* spp. However, the authors concluded that microbes do not play a role in ooid formation based on stable isotopic and trace element results [11]. There were no microborings or microfossils found in the Qaidam Basin Holocene ooids that would have indicated the presence of microbes during ooid formation. Nevertheless, the presence of microbes does not confirm their role in carbonate precipitation as was the case in the study by Duguid et al. [11]. In addition, the positive $\delta^{18}O$ values most likely suggest an authigenic crystallization process driven by intensive evaporation of lake waters, an abiotic process. The progressive ^{18}O

enrichment in the waters during evaporation would drive ^{18}O-enrichment during mineral precipitation [57,58]. The $\delta^{13}C$ values of carbonates may elucidate the abiotic or biotic mechanisms governing their precipitation [29,52,57]. Horton et al. [59] reported a review on globally distributed Quaternary lake carbonate stable isotopic records and modern water isotopic compositions from western North America that suggest the isotopic fractionations associated with lake water evaporation results in the heavy oxygen and carbon isotope enrichment observed in most lakes and lake carbonate records. The $\delta^{13}C$ values of primary carbonates in closed lakes generally ranged from −5‰ to +3‰ [60,61]. The positive $\delta^{13}C$ values of ooids in this study are similar to those of hypersaline carbonates in evaporative environments [29]; however, biologically formed ooids tend to have negative carbon isotopes [52]. Microbial activities tend to preferentially assimilate light carbon isotopes during microbial mineralization, and the precipitated carbonates under this condition will be more depleted in ^{13}C [62,63]. The organic matter formed during photosynthesis from atmospheric CO_2 or HCO_3^- dissolved in water is highly depleted in ^{13}C due to the plants preferentially fixing ^{12}C, which is an indicator for the biogenic origin of carbonates. Stiller et al. [64] suggest that significant ^{13}C enrichment in dissolved inorganic carbon of Dead Sea brines likely resulted from Rayleigh distillation of volatile CO_2 under acidic conditions; however, this process is ineffective in an environment with authigenic carbonate formation [65]. Otherwise, microscopic observations of the ooids show no microfossils or other indication of microbial activity (Figure 5). Margolis and W.Rex [66] also suggested that microbes did not directly relate to aragonitic ooid formation. In the absence of an efficient carbonate-inducing metabolic pathway, we suggest that microorganisms did not play an active role in aragonitic ooids formation. In addition, modern aragonitic ooids are always found in the environment where $CaCO_3$ precipitation was driven by the strong loss of CO_2 from warm and shallow waters [15], which thus leads to a high $\delta^{13}C$ value of ooids. The parallel increase in $\delta^{13}C$ and $\delta^{18}O$ values of the ooids suggest an evaporation process associated with CO_2 degassing, and ooid formation occurring abiotically by increasing alkalinity in a highly evaporative environment.

5.3. Depositional Model for Abiotic Ooids in the Qaidam Basin

In generally, the growth of ooid carbonate cortices occurs in three stages: suspension growth, resting, and sleeping stages [16]. Alternatively, Duguid et al. [11] suggested two life stages: an active stage and a stationary stage. The authors suggest that ooid formation possibly involves the initial precipitation of ACC in the form of microspherules that precipitate on ooid surfaces that transform into aragonite needles typical of tangential ooids [11,16] (Figure 8). During the active stage, the coarse and fine sand at the lake shore can be easily stirred up under strong hydrodynamic conditions. The transient suspension of sediment in lake waters, and then the carbonates, possibly beginning as an ACC veneer, can precipitate at the surface of these sands. Under this condition, ooid growth occurs at the sediment–water interface, while ooids roll in response to the turbulent hydrodynamic conditions [2,11,14,15,19,67]. The deposition rate of carbonate particles is accelerated at this stage, and the $CaCO_3$ saturated waters precipitated around the irregular dark laminae of the ooids, forming the light laminae that primarily consist of microspary carbonate. Then, the ACC transforms into aragonite during the stationary stage, and it is not necessary for ooids to be buried in the subsurface for recrystallization, which was the so-called "sleeping stage" in the model proposed by Davies et al. [16]. Recrystallization of ACC in the stationary stage allows the growth of delicate, radially oriented crystals. The crystallization of aragonite with both abiotic and biotic origin is usually proceeded by the formation and subsequent transformation of ACC [68–70]. Morse et al. [70] observed ACC precipitating on grain surface, and Diaz et al. [13] confirmed the presence of ACC in ooids by the methods of of $^{13}C^1H$ crosspolarization magic-angle spinning nuclear magnetic resonance (CPMAS-NMR) and SEM observations. However, the precipitation of ACC always requires more stringent conditions (e.g., extremely high calcium contents) without bacterial-induced precipitation [69,71], and no ACC was observed in this study.

Although there are numerous studies suggesting a microbial role in ooids formation, an abiotic origin emphasizes that the ooid cortices directly precipitate on a nucleus from supersaturated solution with respect to $CaCO_3$ under the turbulent condition [11,15]. This proposed abiotic mode requires (i) the presence of a nucleus, (ii) water that is supersaturated with respect to calcium carbonate, and (iii) a relatively turbulent environment [11,15,19,72]. In addition, Sorby [73] proposed a "snowball theory" in which ooids are abiotically formed, but organic coatings act as adhesive agents. Similarly, Davies et al. [16] and Bathurst [1] suggested an inorganic precipitation process of ooids via organic surface reactivation. Furthermore, Suess et al. [74] suggested the humic acid dissolved in solution promoted the precipitation of aragonitic ooids. However, radial-concentric ooids have been successfully developed from supersaturated solutions in turbulence environments without any organic contributions [15]. In this study, the dark laminae in ooids samples actively respond to exciting light, but non- and very weak fluorescence within light laminae (Figure 6), which most likely resulted from the presence of trapped aromatic hydrocarbons in the ooid cortices [75], probably indicating the potential role of organic matter in the formation of the aragonitic ooids.

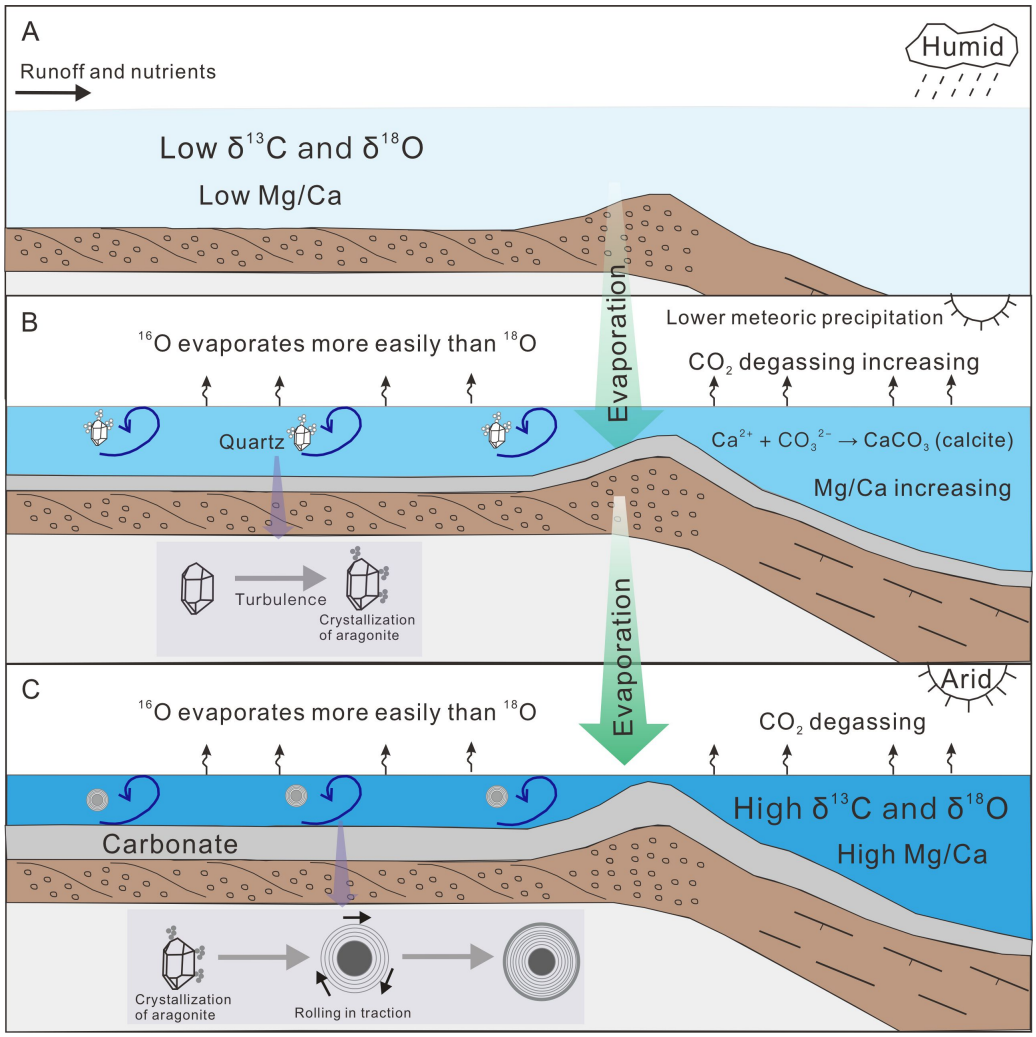

Figure 8. Proposed depositional model for ooids in this study. (**A**) Conceptual diagram illustrating abiotic ooid formation process in an alkaline lake resulting in positive $\delta^{13}C$ and $\delta^{18}O$ values; (**B**) coarse and fine sand is stirred up as a transient suspension in lake waters. Ooid cortices directly precipitate on a nucleus from waters supersaturated with respect to aragonite in a turbulent environment; (**C**) the tangential aragonite crystals (usually minute needle-like) are broken, flattened, and smoothed due to turbulence.

Aragonite and calcite are common carbonate minerals in alkaline lakes; however, their precipitation is the result of complex factors, such as lake water chemistry, ionic interactions, temperature, environment, and EPS in addition to kinetic microbial processes [53,55,57,58,68,76,77]. In this study, there is no evidence of microorganisms participating in the ooid formation or the presence of microbial biofilms (Figure 5), suggesting that microorganisms likely do not significantly contribute to carbonate saturation in the lake. Thus, the abiotic origin of ooids was considered certain, and, although we can not fully exclude any biological influences, abiotic processes are likely the main drivers in ooid formation in this environment. Alkalinity is the dominant factor controlling carbonate precipitation in addition to the content of Ca^{2+} and Mg^{2+}, which could be continuously enriched by intensive evaporation before carbonate precipitation [77,78]. However, temperature and the Mg/Ca ratios are the two controlling factors on $CaCO_3$ mineralogy [53,79]. The precipitation of calcite and aragonite is strongly associated with the Mg/Ca ratios, and increasing Mg/Ca ratio in solution will inhibit calcite formation due to the high kinetic barrier of Mg dehydration, resulting in only aragonite precipitation [76,80–83]. Past seawater chemistry modeling indicates a switch from a calcite sea to aragonite sea during a time when the Mg/Ca value ranged from 1 to 2 [80]. In addition, experimental studies have shown that aragonite tends to precipitate instead of calcite at an Mg/Ca ratio of greater than ∼1.3 [81]. Microbial activity/byproducts, such as polysaccharides, EPS, and possibly amino acids, can promote calcite formation at high Mg/Ca conditions [84,85]. However, in the case of abiotic synthesis, the dissolved silica appears to be the only compound known so far that can promote calcite formation when Mg/Ca ratios are high [84]. Otherwise, the giant ooids in Neoproterozoic were thought to form under an extreme warmth environment (>35 °C) [86]. The occurrence of giant ooids in the Cambrian and Lower Triassic is closely related to the aragonite and/or bimineralic seas and elevated sea-surface temperature [87–90]. The supersaturation of lake water with respect to aragonite was promoted by the increasing evaporation and high Mg/Ca ratio, which are most like regulated by seasonal changes in water chemistry [53,91].

The substructures of ooids most likely resulted from the variable water turbulence [11,15,16]. The radial-fibrous ooids generally occur in quiet or poorly agitated environments, while radial-concentric ooids develop essentially in high-energy environments [11,15,16,92,93]. Most of the ooids in this study are made of a concentric structure and are attributed to nearly continuous bottom agitation in a supersaturated water environment [15]. In high-energy environments (e.g., lake shore), coarse and fine sand was easily stirred up, and then transient suspension in lake waters as the nucleus of ooids. The nucleus of ooids in this study was mainly quartz with minor feldspar and clays (Figures 3 and 5). Aragonite precipitates on the surface of the nucleus under hydrochemical conditions favoring its precipitation with the nucleus being any small solid particle (e.g., sand grain, piece of shell, etc.). Finally, the tangential aragonite crystals are broken, flattened, and smoothed in the turbulence environment. However, in this study, the tangential aragonite crystal (usually minute needle-like) can be observed clearly around the nucleus, indicating the aragonite nucleation and growth quickly in the supersaturated condition.

6. Conclusions

The well-preserved lacustrine aragonitic ooids occur in a playa of the west Qaidam Basin, Western QTP, and provide new insights into the origin and formation processes of carbonate ooids. Radiocarbon dating suggests the exact dates of ooid formation are around 5377 ± 61 cal BP based on radiocarbon dating. Microscopic and mineralogical analyses revealed that ooid cortices were composed of microcrystalline aragonite, with most nuclei being quartz grains. Furthermore, cortices did not contain any microfossils or remnants of microbial activity. Stable carbon and oxygen isotopic data also support inorganic aragonite precipitation with microbes not playing a primary role in the ooid formation. High $\delta^{13}C$ and $\delta^{18}O$ values signature of ooid samples suggest a supergene formation in which authigenic aragonite crystallization from evaporating water is the dominant precipitation process. The

negligible Ce anomalies and negative Eu anomalies of the ooids indicated a predominantly reducing environment for ooid formation without any contribution from hydrothermal activity. Overall, our findings suggest that aragonite ooids with abiotic origin form in a turbulent and aragonite-supersaturated environment (e.g., high Mg/Ca ratio).

Author Contributions: Conceptualization, Y.L., I.M.P. and W.C.; methodology, Y.L. and I.M.P.; investigation, W.C.; writing—original draft preparation, Y.L., I.M.P. and W.C.; writing—review and editing, Y.L., I.M.P. and W.C.; funding acquisition, W.C. and Y.L. All authors have read and agreed to the published version of the manuscript.

Funding: This research is supported by Enterprise Collaboration Project (Investigation on Comprehensive Metallogenic Conditions of Volcanic Sedimentary Boron Deposits in Xiongba Area, Geji County; Grant No. HE1304), and National Natural Science Foundation of China (Grant No. 42102115)

Data Availability Statement: Not applicable.

Conflicts of Interest: The authors declare no conflict of interest.

References

1. Bathurst, R.G. *Carbonate Sediments and Their Diagenesis*; Elsevier: Amsterdam, The Netherlands, 1972.
2. Wilkinson, B.H.; Pope, B.N.; Owen, R.M. Nearshore ooid formation in a modern temperate region marl lake. *J. Geol.* **1980**, *88*, 697–704. [CrossRef]
3. Peryt, T.M. Classification of coated grains. In *Coated Grains*; Springer: Berlin/Heidelberg, Germany, 1983; pp. 3–6.
4. Cohen, A.S.; Thouin, C. Nearshore carbonate deposits in Lake Tanganyika. *Geology* **1987**, *15*, 414–418. [CrossRef]
5. Plee, K.; Ariztegui, D.; Sahan, E.; Martini, R.; Davaud, E. Microbes caught in the act: Disentangling the role of biofilms in the formation of low Mg calcite ooids in a freshwater lake. In Proceedings of the AGU Fall Meeting Abstracts, San Francisco, CA, USA, 14–18 December 2006; Volume 2006, p. B11A-1000.
6. Davaud, E.; Girardclos, S. Recent freshwater ooids and oncoids from western Lake Geneva (Switzerland): Indications of a common organically mediated origin. *J. Sediment. Res.* **2001**, *71*, 423–429. [CrossRef]
7. Tucker, M.E. Calcitized aragonite ooids and cements from the late Precambrian Biri Formation of southern Norway. *Sediment. Geol.* **1985**, *43*, 67–84. [CrossRef]
8. Kenneth Torrance, J.; Kirkpatrick, R. Detrital ooids of Holocene age in glaciomarine Champlain sea sediments, Gatineau, Quebec, Canada. *Can. J. Earth Sci.* **2004**, *41*, 765–773. [CrossRef]
9. Siahi, M.; Hofmann, A.; Master, S.; Mueller, C.; Gerdes, A. Carbonate ooids of the Mesoarchaean Pongola Supergroup, South Africa. *Geobiology* **2017**, *15*, 750–766. [CrossRef]
10. Rankey, E.C.; Reeder, S.L. Holocene ooids of Aitutaki Atoll, Cook Islands, South Pacific. *Geology* **2009**, *37*, 971–974. [CrossRef]
11. Duguid, S.M.; Kyser, T.K.; James, N.P.; Rankey, E.C. Microbes and ooids. *J. Sediment. Res.* **2010**, *80*, 236–251. [CrossRef]
12. Diaz, M.R.; Swart, P.K.; Eberli, G.P.; Oehlert, A.M.; Devlin, Q.; Saeid, A.; Altabet, M.A. Geochemical evidence of microbial activity within ooids. *Sedimentology* **2015**, *62*, 2090–2112. [CrossRef]
13. Diaz, M.R.; Eberli, G.P.; Blackwelder, P.; Phillips, B.; Swart, P.K. Microbially mediated organomineralization in the formation of ooids. *Geology* **2017**, *45*, 771–774. [CrossRef]
14. Diaz, M.R.; Eberli, G.P. Decoding the mechanism of formation in marine ooids: A review. *Earth-Sci. Rev.* **2019**, *190*, 536–556. [CrossRef]
15. Simone, L. Ooids: A review. *Earth-Sci. Rev.* **1980**, *16*, 319–355. [CrossRef]
16. Davies, P.J.; Bubela, B.; Ferguson, J. The formation of ooids. *Sedimentology* **1978**, *25*, 703–730. [CrossRef]
17. Glunk, C.; Dupraz, C.; Braissant, O.; Gallagher, K.L.; Verrecchia, E.P.; Visscher, P.T. Microbially mediated carbonate precipitation in a hypersaline lake, Big Pond (Eleuthera, Bahamas). *Sedimentology* **2011**, *58*, 720–736. [CrossRef]
18. Harris, P.; Diaz, M.R.; Eberli, G.P. The formation and distribution of modern ooids on Great Bahama Bank. *Annu. Rev. Mar. Sci.* **2019**, *11*, 491–516. [CrossRef] [PubMed]
19. Sumner, D.Y.; Grotzinger, J.P. Numerical modeling of ooid size and the problem of Neoproterozoic giant ooids. *J. Sediment. Res.* **1993**, *63*, 974–982.
20. Sun, Y.; Li, Y.; Li, L.; He, H. Preservation of cyanobacterial UVR-shielding pigment scytonemin in carbonate ooids formed in Pleistocene salt lakes in the Qaidam Basin, Tibetan Plateau. *Geophys. Res. Lett.* **2019**, *46*, 10375–10383. [CrossRef]
21. Xiao, L.; Wang, J.; Dang, Y.; Cheng, Z.; Huang, T.; Zhao, J.; Xu, Y.; Huang, J.; Xiao, Z.; Komatsu, G. A new terrestrial analogue site for Mars research: The Qaidam Basin, Tibetan Plateau (NW China). *Earth-Sci. Rev.* **2017**, *164*, 84–101. [CrossRef]
22. Taylor, M.; Yin, A. Active structures of the Himalayan-Tibetan orogen and their relationships to earthquake distribution, contemporary strain field, and Cenozoic volcanism. *Geosphere* **2009**, *5*, 199–214. [CrossRef]
23. Yin, J.; Zhang, S.; Lu, X.; Wu, Z.; Ju, Y. Controls of the Altyn Tagh Fault on the Early–Middle Miocene sedimentation in the Honggouzi Area, Qaidam Basin, Western China. *J. Asian Earth Sci.* **2019**, *181*, 103908. [CrossRef]

24. Power, I.; Wilson, S.; Dipple, G.; Southam, G. Modern carbonate microbialites from an asbestos open pit pond, Yukon, Canada. *Geobiology* **2011**, *9*, 180–195. [CrossRef] [PubMed]
25. Yang, X.; Zhu, B.; White, P.D. Provenance of aeolian sediment in the Taklamakan Desert of western China, inferred from REE and major-elemental data. *Quat. Int.* **2007**, *175*, 71–85. [CrossRef]
26. Lin, Y.; Zheng, M.; Ye, C.; Power, I.M. Trace and rare earth element geochemistry of Holocene hydromagnesite from Dujiali Lake, central Qinghai–Tibetan Plateau, China. *Carbonates Evaporites* **2019**, *34*, 1265–1279. [CrossRef]
27. Taylor, S.R.; McLennan, S.M. *The Continental Crust: Its Composition and Evolution*; Blackwell Scientific Publication: Hoboken, NJ, USA, 1985.
28. Kamber, B.S.; Webb, G.E. The geochemistry of late Archaean microbial carbonate: Implications for ocean chemistry and continental erosion history. *Geochim. Cosmochim. Acta* **2001**, *65*, 2509–2525. [CrossRef]
29. Lin, Y.; Zheng, M.; Ye, C. Hydromagnesite precipitation in the Alkaline Lake Dujiali, central Qinghai-Tibetan Plateau: Constraints on hydromagnesite precipitation from hydrochemistry and stable isotopes. *Appl. Geochem.* **2017**, *78*, 139–148. [CrossRef]
30. Spötl, C.; Vennemann, T.W. Continuous-flow isotope ratio mass spectrometric analysis of carbonate minerals. *Rapid Commun. Mass Spectrom.* **2003**, *17*, 1004–1006. [CrossRef]
31. Ramsey, C.B. Bayesian analysis of radiocarbon dates. *Radiocarbon* **2009**, *51*, 337–360. [CrossRef]
32. Coplen, T.B.; Kendall, C.; Hopple, J. Comparison of stable isotope reference samples. *Nature* **1983**, *302*, 236–238. [CrossRef]
33. Bellanca, A.; Masetti, D.; Neri, R. Rare earth elements in limestone/marlstone couplets from the Albian-Cenomanian Cismon section (Venetian region, northern Italy): Assessing REE sensitivity to environmental changes. *Chem. Geol.* **1997**, *141*, 141–152. [CrossRef]
34. Li, F.; Webb, G.E.; Algeo, T.J.; Kershaw, S.; Lu, C.; Oehlert, A.M.; Gong, Q.; Pourmand, A.; Tan, X. Modern carbonate ooids preserve ambient aqueous REE signatures. *Chem. Geol.* **2019**, *509*, 163–177. [CrossRef]
35. van Smeerdijk Hood, A.; Wallace, M.W. Extreme ocean anoxia during the Late Cryogenian recorded in reefal carbonates of Southern Australia. *Precambrian Res.* **2015**, *261*, 96–111. [CrossRef]
36. Lu, C.; Li, F.; Oehlert, A.M.; Li, J.; Zou, H. Reconstructing paleoceanographic conditions during the middle Ediacaran: Evidence from giant ooids in South China. *Precambrian Res.* **2020**, *351*, 105945. [CrossRef]
37. Webb, G.E.; Kamber, B.S. Rare earth elements in Holocene reefal microbialites: A new shallow seawater proxy. *Geochim. Cosmochim. Acta* **2000**, *64*, 1557–1565. [CrossRef]
38. Holser, W.T. Evaluation of the application of rare-earth elements to paleoceanography. *Palaeogeogr. Palaeoclimatol. Palaeoecol.* **1997**, *132*, 309–323. [CrossRef]
39. De Carlo, E.H.; Green, W.J. Rare earth elements in the water column of Lake Vanda, McMurdo Dry Valleys, Antarctica. *Geochim. Cosmochim. Acta* **2002**, *66*, 1323–1333. [CrossRef]
40. Pattan, J.; Pearce, N.; Mislankar, P. Constraints in using Cerium-anomaly of bulk sediments as an indicator of paleo bottom water redox environment: A case study from the Central Indian Ocean Basin. *Chem. Geol.* **2005**, *221*, 260–278. [CrossRef]
41. Tostevin, R.; Shields, G.A.; Tarbuck, G.M.; He, T.; Clarkson, M.O.; Wood, R.A. Effective use of cerium anomalies as a redox proxy in carbonate-dominated marine settings. *Chem. Geol.* **2016**, *438*, 146–162. [CrossRef]
42. Sverjensky, D.A. Europium redox equilibria in aqueous solution. *Earth Planet. Sci. Lett.* **1984**, *67*, 70–78. [CrossRef]
43. German, C.R.; Elderfield, H. Application of the Ce anomaly as a paleoredox indicator: The ground rules. *Paleoceanography* **1990**, *5*, 823–833. [CrossRef]
44. Piper, D.Z.; Bau, M. Normalized rare earth elements in water, sediments, and wine: Identifying sources and environmental redox conditions. *Am. J. Anal. Chem.* **2013**, *2013*. [CrossRef]
45. Elderfield, H.; Greaves, M.J. The rare earth elements in seawater. *Nature* **1982**, *296*, 214–219. [CrossRef]
46. Trower, E.J.; Cantine, M.D.; Gomes, M.L.; Grotzinger, J.P.; Knoll, A.H.; Lamb, M.P.; Lingappa, U.; O'Reilly, S.S.; Present, T.M.; Stein, N.; et al. Active ooid growth driven by sediment transport in a high-energy shoal, Little Ambergris Cay, Turks and Caicos Islands. *J. Sediment. Res.* **2018**, *88*, 1132–1151. [CrossRef]
47. Trower, E.J.; Lamb, M.P.; Fischer, W.W. Experimental evidence that ooid size reflects a dynamic equilibrium between rapid precipitation and abrasion rates. *Earth Planet. Sci. Lett.* **2017**, *468*, 112–118. [CrossRef]
48. Tang, D.; Shi, X.; Shi, Q.; Wu, J.; Song, G.; Jiang, G. Organomineralization in Mesoproterozoic giant ooids. *J. Asian Earth Sci.* **2015**, *107*, 195–211. [CrossRef]
49. Harris, P.; Diaz, M.; Eberli, G. Ooids as Archives of Past Conditions. In Proceedings of the 2019 AAPG Annual Convention and Exhibition, San Antonio, TX, USA, 19–22 May 2019.
50. Hao, L.; Tao, H.; Li, S.; Ma, X.; Ji, H.; Qiu, J. Distribution and Controlling Growth Factors of Ooids in Qinghai Lake, Northern Tibet Plateau, China. Front. *Earth Sci.* **2022**, *10*, 824453.
51. Brehm, U.; Krumbein, W.E.; Palinska, K.A. Biomicrospheres generate ooids in the laboratory. *Geomicrobiol. J.* **2006**, *23*, 545–550. [CrossRef]
52. Pacton, M.; Ariztegui, D.; Wacey, D.; Kilburn, M.R.; Rollion-Bard, C.; Farah, R.; Vasconcelos, C. Going nano: A new step toward understanding the processes governing freshwater ooid formation. *Geology* **2012**, *40*, 547–550. [CrossRef]
53. Dupraz, C.; Reid, R.P.; Braissant, O.; Decho, A.W.; Norman, R.S.; Visscher, P.T. Processes of carbonate precipitation in modern microbial mats. *Earth-Sci. Rev.* **2009**, *96*, 141–162. [CrossRef]

54. O'reilly, S.; Mariotti, G.; Winter, A.; Newman, S.; Matys, E.; McDermott, F.; Pruss, S.; Bosak, T.; Summons, R.; Klepac-Ceraj, V. Molecular biosignatures reveal common benthic microbial sources of organic matter in ooids and grapestones from Pigeon Cay, The Bahamas. *Geobiology* **2017**, *15*, 112–130. [CrossRef]
55. Castanier, S.; Le Métayer-Levrel, G.; Perthuisot, J.P. Ca-carbonates precipitation and limestone genesis—The microbiogeologist point of view. *Sediment. Geol.* **1999**, *126*, 9–23. [CrossRef]
56. Plee, K.; Ariztegui, D.; Martini, R.; Davaud, E. Unravelling the microbial role in ooid formation–results of an in situ experiment in modern freshwater Lake Geneva in Switzerland. *Geobiology* **2008**, *6*, 341–350. [CrossRef]
57. Cangemi, M.; Censi, P.; Reimer, A.; D'Alessandro, W.; Hause-Reitner, D.; Madonia, P.; Oliveri, Y.; Pecoraino, G.; Reitner, J. Carbonate precipitation in the alkaline lake Specchio di Venere (Pantelleria Island, Italy) and the possible role of microbial mats. *Appl. Geochem.* **2016**, *67*, 168–176. [CrossRef]
58. Power, I.M.; Harrison, A.L.; Dipple, G.M.; Wilson, S.A.; Barker, S.L.; Fallon, S.J. Magnesite formation in playa environments near Atlin, British Columbia, Canada. *Geochim. Cosmochim. Acta* **2019**, *255*, 1–24. [CrossRef]
59. Horton, T.W.; Defliese, W.F.; Tripati, A.K.; Oze, C. Evaporation induced 18O and 13C enrichment in lake systems: A global perspective on hydrologic balance effects. *Quat. Sci. Rev.* **2016**, *131*, 365–379. [CrossRef]
60. McKenzie, J.A. Carbon isotopes and productivity in the lacustrine and marine environment. *Chem. Process. Lakes* **1985**, 99–118.
61. Talbot, M. A review of the palaeohydrological interpretation of carbon and oxygen isotopic ratios in primary lacustrine carbonates. *Chem. Geol. Isot. Geosci. Sect.* **1990**, *80*, 261–279. [CrossRef]
62. Luzón, A.; Mayayo, M.; Pérez, A. Stable isotope characterisation of co-existing carbonates from the Holocene Gallocanta lake (NE Spain): Palaeolimnological implications. *Int. J. Earth Sci.* **2009**, *98*, 1129–1150. [CrossRef]
63. Hips, K.; Haas, J.; Poros, Z.; Kele, S.; Budai, T. Dolomitization of Triassic microbial mat deposits (Hungary): Origin of microcrystalline dolomite. *Sediment. Geol.* **2015**, *318*, 113–129. [CrossRef]
64. Stiller, M.; Rounick, J.; Shasha, S. Extreme carbon-isotope enrichments in evaporating brines. *Nature* **1985**, *316*, 434–435. [CrossRef]
65. Birgel, D.; Meister, P.; Lundberg, R.; Horath, T.; Bontognali, T.R.; Bahniuk, A.M.; de Rezende, C.E.; Vásconcelos, C.; McKenzie, J.A. Methanogenesis produces strong 13C enrichment in stromatolites of Lagoa Salgada, Brazil: A modern analogue for Palaeo-/Neoproterozoic stromatolites? *Geobiology* **2015**, *13*, 245–266. [CrossRef]
66. Margolis, S.; Rex, R.W. Endolithic algae and micrite envelope formation in Bahamian oölites as revealed by scanning electron microscopy. *Geol. Soc. Am. Bull.* **1971**, *82*, 843–852. [CrossRef]
67. Tan, Q.; Shi, Z.J.; Tian, Y.M.; Wang, Y.; Wang, C.C. Origin of ooids in ooidal-muddy laminites: A case study of the lower Cambrian Qingxudong Formation in the Sichuan Basin, South China. *Geol. J.* **2018**, *53*, 1716–1727. [CrossRef]
68. Obst, M.; Dynes, J.J.; Lawrence, J.R.; Swerhone, G.D.; Benzerara, K.; Karunakaran, C.; Kaznatcheev, K.; Tyliszczak, T.; Hitchcock, A.P. Precipitation of amorphous $CaCO_3$ (aragonite-like) by cyanobacteria: A STXM study of the influence of EPS on the nucleation process. *Geochim. Cosmochim. Acta* **2009**, *73*, 4180–4198. [CrossRef]
69. Bots, P.; Benning, L.G.; Rodriguez-Blanco, J.D.; Roncal-Herrero, T.; Shaw, S. Mechanistic insights into the crystallization of amorphous calcium carbonate (ACC). *Cryst. Growth Des.* **2012**, *12*, 3806–3814. [CrossRef]
70. Morse, J.W.; Mackenzie, F.T. *Geochemistry of Sedimentary Carbonates*; Elsevier: Amsterdam, The Netherlands, 1990.
71. Enyedi, N.T.; Makk, J.; Kótai, L.; Berényi, B.; Klébert, S.; Sebestyén, Z.; Molnár, Z.; Borsodi, A.K.; Leél-Őssy, S.; Demény, A.; et al. Cave bacteria-induced amorphous calcium carbonate formation. *Sci. Rep.* **2020**, *10*, 1–12. [CrossRef]
72. Rankey, E.C.; Reeder, S.L. Tidal sands of the Bahamian archipelago. In *Principles of Tidal Sedimentology*; Springer: Berlin/Heidelberg, Germany, 2012; pp. 537–565.
73. Sorby, H.C. The structure and origin of limestones. *Pop. Sci. Rev.* **1879**, *3*, 134–137.
74. Suess, E.; Fütterer, D. Aragonitic ooids: Experimental precipitation from seawater in the presence of humic acid. *Sedimentology* **1972**, *19*, 129–139. [CrossRef]
75. Pedone, V.A.; Cercone, K.R.; Burruss, R. Activators of photoluminescence in calcite: Evidence from high-resolution, laser-excited luminescence spectroscopy. *Chem. Geol.* **1990**, *88*, 183–190. [CrossRef]
76. De Choudens-Sanchez, V.; Gonzalez, L.A. Calcite and aragonite precipitation under controlled instantaneous supersaturation: elucidating the role of $CaCO_3$ saturation state and Mg/Ca ratio on calcium carbonate polymorphism. *J. Sediment. Res.* **2009**, *79*, 363–376. [CrossRef]
77. Balci, N.; Demirel, C.; Ön, S.A.; Gültekin, A.H.; Kurt, M.A. Evaluating abiotic and microbial factors on carbonate precipitation in Lake Acigöl, a hypersaline lake in Southwestern Turkey. *Quat. Int.* **2018**, *486*, 116–128. [CrossRef]
78. Belmaker, R.; Lazar, B.; Stein, M.; Taha, N.; Bookman, R. Constraints on aragonite precipitation in the Dead Sea from geochemical measurements of flood plumes. *Quat. Sci. Rev.* **2019**, *221*, 105876. [CrossRef]
79. Burton, E.A.; Walter, L.M. Relative precipitation rates of aragonite and Mg calcite from seawater: Temperature or carbonate ion control? *Geology* **1987**, *15*, 111–114. [CrossRef]
80. Wilkinson, B.H. Sedimentary carbonate record of calcium-magnesium cycling. *Am. J. Sci.* **1989**, *289*, 1158–1194. [CrossRef]
81. Morse, J.W.; Wang, Q.; Tsio, M.Y. Influences of temperature and Mg: Ca ratio on $CaCO_3$ precipitates from seawater. *Geology* **1997**, *25*, 85–87.
82. Ries, J.B. Effect of ambient Mg/Ca ratio on Mg fractionation in calcareous marine invertebrates: A record of the oceanic Mg/Ca ratio over the Phanerozoic. *Geology* **2004**, *32*, 981–984. [CrossRef]

83. Rossi, C.; Lozano, R.P. Hydrochemical controls on aragonite versus calcite precipitation in cave dripwaters. *Geochim. Cosmochim. Acta* **2016**, *192*, 70–96.
84. Fang, Y.; Xu, H. Dissolved silica-catalyzed disordered dolomite precipitation. *Am. Mineral. J. Earth Planet. Mater.* **2022**, *107*, 443–452.
85. Lin, C.Y.; Turchyn, A.V.; Steiner, Z.; Bots, P.; Lampronti, G.I.; Tosca, N.J. The role of microbial sulfate reduction in calcium carbonate polymorph selection. *Geochim. Cosmochim. Acta* **2018**, *237*, 184–204. [CrossRef]
86. Trower, E.J. The enigma of Neoproterozoic giant ooids—Fingerprints of extreme climate? *Geophys. Res. Lett.* **2020**, *47*, e2019GL086146.
87. Koeshidayatullah, A.; Trower, E.J.; Li, X.; Mukerji, T.; Lehrmann, D.J.; Morsilli, M.; Al-Ramadan, K.; Payne, J.L. Quantitative evaluation of the roles of ocean chemistry and climate on ooid size across the Phanerozoic: Global versus local controls. *Sedimentology* **2022**, *69*, 2486–2506.
88. Li, F.; Gong, Q.; Burne, R.V.; Tang, H.; Su, C.; Zeng, K.; Zhang, Y.; Tan, X. Ooid factories operating under hothouse conditions in the earliest Triassic of South China. *Glob. Planet. Change* **2019**, *172*, 336–354.
89. Lehrmann, D.J.; Minzoni, M.; Li, X.; Yu, M.; Payne, J.L.; Kelley, B.M.; Schaal, E.K.; Enos, P. Lower Triassic oolites of the Nanpanjiang Basin, south China: Facies architecture, giant ooids, and diagenesis—Implications for hydrocarbon reservoirsGeologic Note. *AAPG Bull.* **2012**, *96*, 1389–1414. [CrossRef]
90. Chow, N.; James, N.P. Facies-specific, calcitic and bimineralic ooids from Middle and Upper Cambrian platform carbonates, western Newfoundland, Canada. *J. Sediment. Res.* **1987**, *57*, 907–921.
91. McCormack, J.; Nehrke, G.; Jöns, N.; Immenhauser, A.; Kwiecien, O. Refining the interpretation of lacustrine carbonate isotope records: Implications of a mineralogy-specific Lake Van case study. *Chem. Geol.* **2019**, *513*, 167–183. [CrossRef]
92. Davies, P.J.; Martin, K. Radial aragonite ooids, Lizard Island, great barrier reef, Queensland, Australia. *Geology* **1976**, *4*, 120–122. [CrossRef]
93. Xiao, E.; Riaz, M.; Zafar, T.; Latif, K. Cambrian marine radial cerebroid ooids: Participatory products of microbial processes. *Geol. J.* **2021**, *56*, 4627–4644. [CrossRef]